International Journal on Science and Technology (IJSAT)
E-ISSN: 2229-7677 ● Website: www.ijsat.org ● Email: editor@ijsat.org

Attitude Control and Navigation of Low Earth Orbit Satellite

Seda (Karadeniz) Kartal
sedakaradeniz@gmail.com
ORCID: https://orcid.org/0000-0003-4756-5490
Address: Bahçelievler Mahallesi, 138 Cadde, No:33/13, Gölbaşı, Ankara, Türkiye

Abstract
In this study, the orbit and attitude model of a low Earth orbit satellite has been developed. The attitude model is addressed both dynamically and kinematically, and the quaternion parameters and Euler angles of the satellite are obtained. Noise is added to this attitude information to generate sensor data for the INS (Inertial Navigation System) and GPS (Global Positioning System). The attitude information is estimated by combining the two-sensor data with INS/GPS integrated navigation system using an Extended Kalman Filter algorithm. To control the satellite's attitude, a DC motor model driving the reaction wheels is created, and the angular velocity and torque of the motor are controlled. A PID controller is designed for satellite attitude control. The optimal gain coefficients of the PID controller are determined by minimizing the difference between the integrated navigation system output and the desired attitude information. By generating reference inputs for the satellite model, the satellite's attitude is controlled. The results show that in the integrated system, consisting of satellite orbit, attitude model, navigation, and control design, the satellite reaches the desired attitude quickly and stably. The entire study is carried out in the MATLAB/Simulink environment.

Keywords: Low Earth Orbit Satellite, Control, Navigation, INS/GPS integration, PID

1. Introduction

Satellites are classified into three main categories based on their orbits: low Earth orbit (LEO), medium Earth orbit (MEO), and geostationary Earth orbit (GEO). LEO satellites are located at an altitude between 160 km and 2,000 km and are generally used for short-range missions such as communication, imaging, weather observations, and scientific research [1]. MEO satellites operate in orbits ranging from 2,000 km to 35,786 km and are particularly ideal for global navigation systems such as GPS. GEO satellites, on the other hand, orbit above 35,786 km, maintaining a trajectory parallel to the Earth's rotation speed, and are primarily used for long-term, wide-area services such as fixed communication, weather observations, and television broadcasting [2]. Each orbital type has specific characteristics optimized for particular missions and applications.

In this study, the low Earth orbit satellite Flying Laptop, developed by the Institute of Space Systems at the University of Stuttgart, is examined. The satellite weighs 120 kg, measures 60 cm × 70 cm × 80 cm,

and operates at an altitude between 500 km and 900 km in low Earth orbit, primarily for space research and technological testing purposes. For LEO satellites to operate successfully, both control and navigation systems must function with high accuracy. Satellites require an effective navigation and control system to align with their orbits and maintain the desired attitude[3]. These systems integrate data from various sensors such as gyroscopes and accelerometers for inertial navigation, as well as magnetometers, GPS, star trackers, and sun sensors to accurately determine the satellite's position and orientation. As demonstrated in the work of Farhangian et al., integrating INS and GPS systems is particularly suitable for such missions as it ensures continuous and precise positioning, especially for moving platforms [4]. Furthermore, Prol et al. provide a comprehensive review indicating that while the positioning, navigation, and timing (PNT) needs of LEO satellites are met with current technologies, significant research opportunities remain regarding challenges and future developments [5].

In recent years, optical navigation has also gained attention for application in LEO satellites. The study by Hu et al. discusses the design of sensor scheduling strategies for optical navigation systems, emphasizing their potential to improve accuracy in satellite missions [6]. However, while each of these sensors provides unique advantages, they may not be sufficient on their own. For example, inertial navigation systems offer short-term accuracy but suffer from drift over time. To address this issue, the Kalman filter integrates data from INS and GPS, performing error corrections to ensure highly accurate position and orientation estimation. Additionally, as highlighted in the study by Ye et al., integrated algorithms developed for LEO satellites have the potential to provide continuous and accurate position information even during GPS signal outages [7].

The integration of navigation and control systems also brings significant advantages, particularly for complex missions such as formation flying, as discussed by Ivanov et al. [8]. These integrations enhance mission efficiency and enable more reliable operations for LEO satellites under dynamic conditions. In this context, the ESTCube-2 demonstrator, developed by Dalbins et al., serves as an exemplary case for evaluating the performance of such integrated systems [9]. All these studies demonstrate that improving navigation systems enhances the reliability and effectiveness of LEO satellites.

The data obtained from navigation systems serve as inputs to control algorithms, ensuring that the satellite remains in the desired orbit and achieves its targeted orientation. Therefore, satellite control design is directly linked to the accuracy and reliability of navigation data. In this context, an effective control system must efficiently utilize the information from the navigation system. Various control methods exist, depending on the mission requirements and the operational environment of the satellite. For instance, in a study by Daniel Calvo and colleagues, a fuzzy logic-based controller was designed for the attitude control of a nano-satellite in low Earth orbit, demonstrating improvements in attitude accuracy [10]. Similarly, Boussadia et al. proposed a sliding mode control strategy based on the backstepping approach for attitude determination and control of microsatellites, achieving high-precision attitude control [11]. For more complex missions, such as formation flying, Ivanov et al. developed a decentralized control approach for tetrahedral formation flying of nano-satellites, leveraging aerodynamic forces [12]. Additionally, Sandu et al. introduced a novel solar-thermal/cold gas propulsion system for attitude control of LEO satellites, offering an innovative control solution [13]. More conventional methods, such as the study by Avanzini et al., explore the combined use of reaction wheels and magnetic torque rods for attitude control in low Earth orbit, demonstrating the performance benefits of this hybrid approach [14]. Moreover, H. A. Talebi and colleagues developed a recurrent neural network-based method for sensor and actuator fault detection and isolation, providing a viable solution for satellite attitude control subsystems [15].

The aforementioned control methods offer diverse approaches and advantages for satellite attitude control. However, one of the most fundamental and widely used techniques in satellite control systems is the PID (proportional-integral-derivative) controller. Due to its simplicity, ease of implementation, and broad application range, PID controllers are frequently used in attitude control tasks, optimizing torque generation for satellites [16]. A satellite utilizes PID controllers alongside reaction wheels or magnetic torque rods to maintain the desired orientation. Furthermore, PID controllers are often integrated with Kalman filters or other sensor fusion techniques to ensure a highly accurate balance between navigation and control systems. These features make PID controllers a fundamental tool for satellite attitude control. However, for more complex and precise control applications, cascade control or model-based control techniques may be preferred [17].

In this study, an integrated navigation system and attitude controller were designed for a low Earth orbit satellite. The satellite's attitude information was generated through a mathematical model based on both kinematic and dynamic formulations. Sensor measurement data were simulated by adding noise to the model-based generated data. Using the dynamic equations of the onboard INS, a Kalman filter-based INS/GPS integrated navigation system was developed. In this system, model-generated sensor data formed the measurement model of the extended Kalman filter algorithm, while the INS dynamic equations formed the system model. The output of the integrated navigation system and reference attitude information were used as inputs to the attitude controller. Using an attitude controller alone was insufficient to fully regulate the satellite's orientation. Therefore, a cascade controller was designed to regulate the angular speed and torque of four reaction wheels onboard the satellite. The attitude controller generated a reference angular velocity for the reaction wheels, while the reaction wheel controller produced reference torque commands for the satellite attitude model. Consequently, an integrated system was developed that estimates the satellite's attitude using sensor data, implements a Kalman filter-based navigation system, and utilizes navigation information to generate the required reference orientation through attitude and reaction wheel controllers.

The paper is structured as follows: Section 2 presents the satellite orbit model. Section 3 explains the satellite attitude model, which consists of kinematic and dynamic components. Section 4 focuses on satellite attitude control, specifically the control of reaction wheel torques and angular velocities. Section 5 describes the integrated navigation system, detailing the Kalman filter-based INS/GPS navigation model. Finally, the paper is concluded in Section 6.

2. Orbit Propagation Model of Low Earth Orbit Satellite

Satellite orbits can be determined using classical methods based on Newton's laws, Keplerian orbit calculations, and Gauss's methods. More modern approaches provide real-time orbit prediction and error correction using Kalman filters, digital integration methods, and astrodynamics models. One of the data-based methods for orbit determination is the use of TLE (Two-Line Element) data.TLE is a data format that defines a satellite's orbital elements in a two-line format and is typically obtained from sources such as NORAD, CelesTrak, and ISS Tracker. In this study, the TLE data of the Flying Laptop low Earth orbit satellite were used for the orbit propagation model [18], [19]. From the TLE data, Keplerian parameters such as eccentricity (e), inclination angle (i), mean motion (n), mean anomaly (M), argument of perigee

(w), and right ascension of the ascending node (Ω) were extracted, while unknown parameters such as the semi-major axis (a) and the mean semi-latus rectum (p) were calculated.

The relationship between the mean anomaly (n) and the semi-major axis, as well as the relationship between the mean semi-latus rectum (p), eccentricity, and the semi-major axis, is given inEquation 1. Using Equation 1, the values of the semi-major axis and the semi-latus rectum were calculated [20], [21].

$$n = \sqrt{\frac{\mu}{a^3}}, \quad T = \frac{2\pi}{n}, p = a(1 - e^2) \tag{1}$$

The eccentric anomaly (E) is obtained using the Newton-Raphson method. The true anomaly (θ) of the satellite is calculated using Equations 2 and 3.

$$\sin(\theta) = \frac{\sqrt{1 - e^2} sinE}{1 - e.cosE} \tag{2}$$

$$\cos(\theta) = \frac{cosE - e}{1 - e.cosE}, \theta = \arctan\left(\frac{sin\theta}{cos\theta}\right) \tag{3}$$

The magnitude of the satellite position vector is calculated using Equation 4[21].

$$r = \frac{p}{1 + e.\cos(\theta)} = \frac{a(1 - e^2)}{1 + e.\cos(\theta)} \tag{4}$$

The position and velocity information of the satellite in the orbital frame is obtained as given in Equation 5.

$$R^o = \begin{bmatrix} R_x^o \\ R_y^o \\ R_z^o \end{bmatrix} = \begin{bmatrix} r.\cos(\theta) \\ r.sin(\theta) \\ 0 \end{bmatrix}, V^o = \begin{bmatrix} V_x^o \\ V_y^o \\ V_z^o \end{bmatrix} = \begin{bmatrix} -\sqrt{\mu/p}.\cos(\theta) \\ \sqrt{\mu/p}.(e + \cos(\theta) \\ 0 \end{bmatrix} \tag{5}$$

To obtain the position and velocity information of the satellite in the Earth-Centered Inertial (ECI) frame from its position and velocity in the orbital frame, the transformation matrix J, defined as in Equation 6, is used [21].

$$J = \begin{bmatrix} J_{11} & J_{12} & J_{13} \\ J_{21} & J_{22} & J_{23} \\ J_{31} & J_{R32} & J_{33} \end{bmatrix} \tag{6}$$

where

$J_{11} = \cos(\Omega)\cos(w) - \sin(\Omega)\sin(w)\cos(i)$

$J_{12} = -\cos(\Omega)\sin(w) - \sin(\Omega)\cos(w)\cos(i)$

$J_{13} = \sin(\Omega)\sin(i)$

$J_{21} = \sin(\Omega)\cos(w) + \cos(\Omega)\sin(w)\cos(i)$

$J_{22} = -\sin(\Omega)\sin(w) + \cos(\Omega)\cos(w)\cos(i)$

$J_{23} = -\cos(\Omega)\sin(i)$

$J_{31} = \sin(w)\sin(i)$

$J_{32} = \cos(w)\sin(i)$

$J_{33} = \cos(i)$

The position and velocity of the satellite in the ECI frame are obtained using Equation 7. All system and measurement data are transformed into the Earth-Centered Earth-Fixed (ECEF) frame for the Extended Kalman Filter[21].

$$R^{ECI} = \begin{bmatrix} x \\ y \\ z \end{bmatrix} = [T] \begin{bmatrix} r.\cos(\theta) \\ r.sin(\theta) \\ 0 \end{bmatrix}, \qquad V^{ECI} = [T] \begin{bmatrix} -\sqrt{\mu/p}.\cos(\theta) \\ \sqrt{\mu/p}.(e + \cos(\theta) \\ 0 \end{bmatrix} \tag{7}$$

The position information of the Flying Laptop satellite in the ECEF frame along the x and y axes is obtained using Equations 8 and 9.

$$R^{ECEF} = [C_z(-\Omega + w_{ie})][C_x(-i)][C_z(-w)][R^O] \tag{8}$$

$$V^{ECEF} = [C_z(-\Omega + w_{ie})][C_x(-i)][C_z(-w)][V^O] \tag{9}$$

Burada

$$C_z(-\Omega + w_{ie}) = \begin{bmatrix} cos(-\Omega + w_{ie}) & sin(-\Omega + w_{ie}) & 0 \\ -sin(-\Omega + w_{ie}) & cos(-\Omega + w_{ie}) & 0 \\ 0 & 0 & 1 \end{bmatrix}$$

$$C_z(-\mathrm{w}) = \begin{bmatrix} cos(-\mathrm{w}) & sin(-\mathrm{w}) & 0 \\ -sin(-\mathrm{w}) & cos(-\mathrm{w}) & 0 \\ 0 & 0 & 1 \end{bmatrix}$$

$$C_x(-i) = \begin{bmatrix} 1 & 0 & 0 \\ 0 & cos((-i)) & sin((-i)) \\ 0 & -sin((-i)) & cos((-i)) \end{bmatrix}$$

In this study, the focus is on the satellite's maneuvering motion rather than its orbit, and the attitude model for satellite attitude control and attitude navigation is developed in the following section.

3. Attitude Model of Low Earth Orbit Satellite

The satellite's attitude model consists of kinematic and dynamic models. The dynamic model addresses the physical forces and interactions, such as torque and momentum, that drive changes in the satellite's attitude. In the satellite's attitude model, the kinematic model describes how the satellite's orientation changes over time using parameters such as quaternions or Euler angles.

3.1. Dynamic Model

The dynamic model describes the derivation of the satellite's angular velocity as follows [21]:

$$\dot{w}_{ib}^{b} = I_s^{-1}\left[T_D - \dot{H}_{RW}^{b} - \Omega\left(w_{ib}^{b}\right)I_s w_{ib}^{b} - \Omega(w_{ib}^{b})H_{RW}^{b}\right] \tag{10}$$

where

I_s; inertia tensor matrix of satellite

T_D; the torque based on perturbations

H_{RW}^{b}; the momentum generated by reaction wheels

$\dot{H}_{RW}^{b}$; the torque produced by reaction wheels, $\dot{H}_{RW}^{b} = T_C$.

w_{ib}^{b}; the angular velocity of satellite in body-frame

$\Omega\left(w_{ib}^{b}\right)$; the skew-symmetric matrix based on angular velocity

The attitude motion of the satellite is influenced by perturbation torques arising from gravity gradient, solar radiation, aerodynamics, and the magnetic dipole moment [20]. This perturbation torques are counteracted using reaction wheels or magnetic torque rods. In this study, the torque generated by reaction wheels is considered as the control torque. Additionally, the perturbation torques are assumed to have a constant value.

The inertia tensor matrix is assumed to be a diagonal matrix because the influence of the off-diagonal elements is negligible[22].

$$I_s = \begin{bmatrix} I_{sxx} & 0 & 0 \\ 0 & I_{syy} & 0 \\ 0 & 0 & I_{szz} \end{bmatrix} \tag{11}$$

The skew-symmetric matrix, derived from the satellite's angular velocity along the x, y, and z axes, is expressed as follows [22]:

$$\Omega(w_{ib}^{b}) = \begin{bmatrix} 0 & -w_{ib,z}^{b} & w_{ib,y}^{b} \\ w_{ib,z}^{b} & 0 & -w_{ib,x}^{b} \\ -w_{ib,y}^{b} & w_{ib,x}^{b} & 0 \end{bmatrix} \quad (12)$$

3.2. Kinematic Model

The kinematic model facilitates the transformation between different reference frames. Using the kinematic model, the satellite's angular velocity is converted from the body frame to the orbit frame. This transformation is typically performed using a transformation matrix composed of Euler angles. However, in this study, the transformation matrix $C(q)_{o}^{b}$, defined by quaternion vectors $[q_1 \quad q_2 \quad q_3 \quad q_4]$, is employed instead of Euler angles, as Euler angles become undefined at certain orientations, particularly at 90 degrees [20]. Kinematic model is expressed as follows:

$$\dot{q} = \frac{1}{2}\Omega(w_{ob}^{b})q \quad (13)$$

where $\Omega(w_{ob}^{b})$represents the skew-symmetric matrix corresponding to the satellite's angular velocity in the orbit frame, and it is derived as follows [20]:

$$\begin{bmatrix} w_x \\ w_y \\ w_z \end{bmatrix}_{ob}^{b} = \begin{bmatrix} w_x \\ w_y \\ w_z \end{bmatrix}_{ib}^{b} - C_{o}^{b} \begin{bmatrix} 0 \\ -w_0 \\ 0 \end{bmatrix} \quad (14)$$

where w_{ob}^{b}denotes the angular velocity of the satellite in the orbit frame w_{ib}^{b}represents the angular velocity of the satellite in the body frame. The satellite's mean motion, denoted by$w_0$is determined as follows:

$$w_0 = \sqrt{\frac{GM_e}{R^3}} \quad (15)$$

G represents the gravitational constant of Earth, Medenotes the Earth's mass, and R refers to the distance between the satellite and Earth. In this study, the value of $w_0$is assumed to be approximately 0.0069 rad/s. The transformation matrix used to convert from the body frame to the orbit frame is defined as follows [20].

$$C(q)_{o}^{b} = \begin{bmatrix} C(q)_{11} & C(q)_{12} & C(q)_{13} \\ C(q)_{21} & C(q)_{22} & C(q)_{23} \\ C(q)_{31} & C(q)_{32} & C(q)_{33} \end{bmatrix} \quad (16)$$

where

Euler angles such as roll, pitch and yaw of the satellite are obtained using the quaternion parameters detailed in [23].

4. Attitude Control of Low Earth Orbit Satellite

The precise and accurate control of a satellite's attitude information is critically important for mission success. While performing tasks such as communication, observation, navigation, or scientific research, the satellite must be directed toward predetermined targets. An incorrect attitude can lead to data loss, signal interruptions, and energy inefficiency. Especially in low Earth orbit, satellites require continuous attitude adjustments due to atmospheric drag and other external influences. In this study, PID controllers were designed to successfully control the attitude of a low Earth orbit satellite using the angular velocity and torque of its reaction wheels.

When the four reaction wheels in the tetrahedral configuration of a low Earth orbit satellite are activated, the satellite undergoes rotational motion along the x-axis (roll), y-axis (pitch), and z-axis (yaw). In this study, the satellite's Euler angles were generated by adding noise to the data obtained from the satellite's attitude mathematical model. These sensor data were estimated using an extended Kalman filter-based INS/GPS integrated navigation system, which serves as the input for the PID attitude controller.

The PID attitude controller minimizes the difference between the reference attitude angle and the estimated attitude angle, determining the optimal gain coefficients for the designed controller and generating the desired reference angular velocity for the reaction wheels. However, designing an attitude controller alone is not sufficient for controlling the satellite's attitude angles. The angular velocity and torque of the DC motors driving the reaction wheels were controlled using cascade PID controllers, ensuring the generation of the required reference torque for the satellite. The block diagram of the entire integrated system for satellite attitude control is presented below.

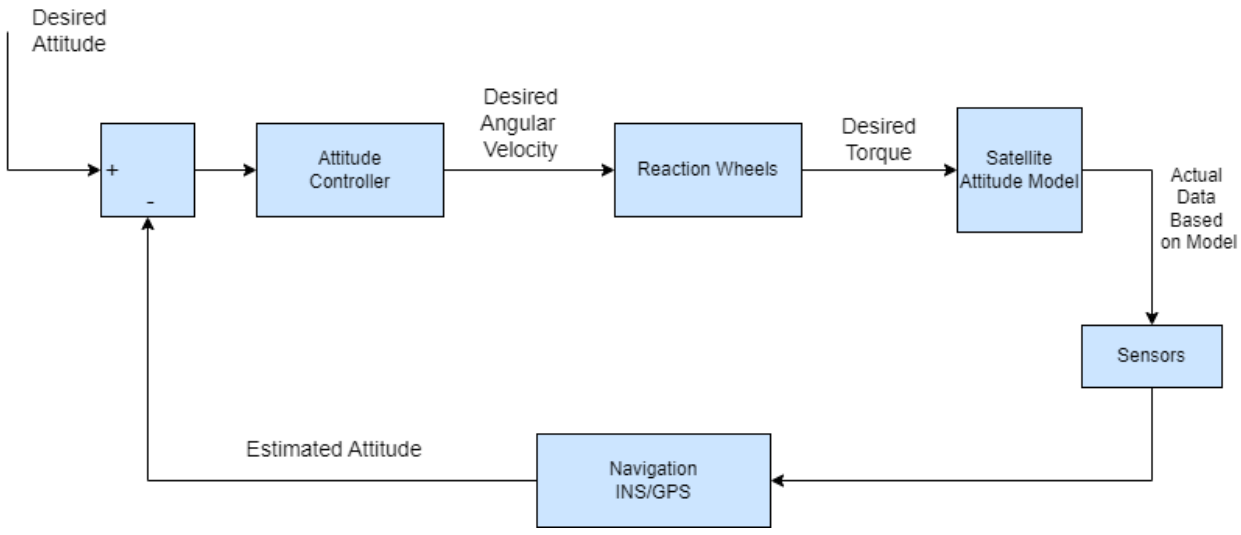

Figure 1. Block diagram of control and navigation system of LEO

5. Reaction Wheel Control

The attitude control of a low Earth orbit satellite is critically important for successfully performing its assigned mission. In this study, four reaction wheels were used to control the attitude of the LEO satellite in roll, pitch, and yaw. These wheels are driven by DC motors. When the reaction wheels are activated, they generate angular velocity, which in turn results in roll, pitch, and yaw angle variations. There are

different configurations of reaction wheels, such as the 3-wheel configuration, 4-wheel redundant configuration, 4-wheel tetrahedral configuration, and 4-wheel off-centered configuration. The choice of configuration affects the performance of the satellite's attitude control. Different configurations influence torque generation capacity, energy consumption, system stabilization speed, stability, and maneuverability [24].

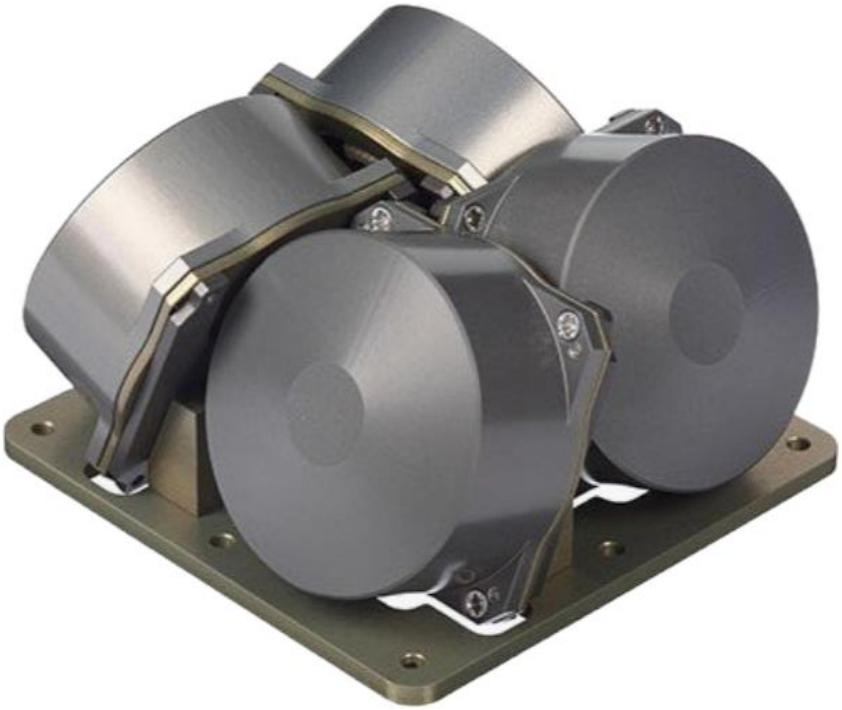

Figure 2. Tetrahedral reaction wheels of FLP [22].

In this study, the 4-wheel off-centered configuration was selected for the reaction wheels, as shown in Figure 2. These wheels are symmetrically placed on the satellite to generate effective torque along each axis. This configuration allows for more precise attitude control by minimizing interactions between the axes, ensuring independent and accurate orientation adjustments.

To determine the torques generated by the reaction wheels, a distribution matrix must be formulated for configurations containing more than three reaction wheels. For the satellite, the allocation problem involves three Euler angles representing roll, pitch, and yaw and four actuators corresponding to the reaction wheels. The allocation matrix L is composed of four column vectors, where each vector defines how the torques generated by the reaction wheels are distributed across the satellite's rotational axes. In this study, the distribution matrix for the four-wheel configuration is defined as [18], [19].

$$L = \begin{bmatrix} r_x^1 & r_x^2 & r_x^3 & r_x^4 \\ r_y^1 & r_y^2 & r_y^3 & r_y^4 \\ r_z^1 & r_z^2 & r_z^3 & r_z^4 \end{bmatrix} \tag{17}$$

In this study, the reaction wheels responsible for the satellite's attitude control are driven by DC motors. To achieve the desired orientation, it is necessary to control both the angular velocities of the motors and

the torque they generate. For this purpose, the DC motors driving the reaction wheels are controlled using a PID controller. A cascade PID control scheme, consisting of inner and outer loops, is implemented to regulate the motors' angular velocity and torque. The DC motor model driving the reaction wheels is presented below.

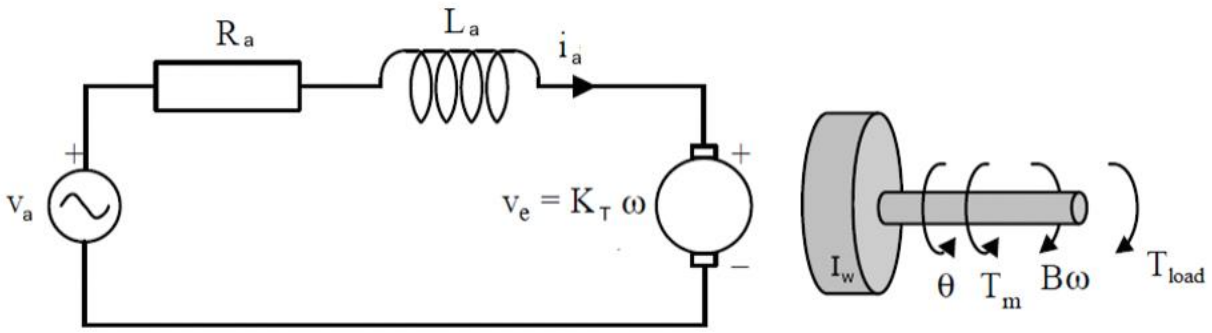

Figure 3. The circuit model of the DC motor driving the reaction wheels [22]

Applying Kirchhoff's Voltage Law to the given DC motor circuit model yields the following equation:

$$L_a \frac{d}{dt} i_a = -R_a i_a - K_E W_{RW} + u_a \tag{18}$$

In a DC motor with a constant magnetic field, the torque generated by the reaction wheels (T_C)or (H_{Rw})and the momentum (H_{Rw}) are directly proportional to the armature current and can be expressed as follows:

$$T_C = \dot{H}_{RW} = K_T i_a = I_W \dot{W}_{RW} + B W_{RW} \tag{19}$$

$$H_{RW} = I_{Rw} W_{Rw} \tag{20}$$

where,

L_a: Armature Inductance (H), R_a: Armature Resistance, $\dot{I}_a$: Input Current (A), V_a: Input Voltage (V), V_e:Input Voltage (V), K_T: Torque Constant (Nm/A), K_E: Field Constant (V/(rad/s)), T_L: Torque Load (Nm), I_w: Reaction Wheel Inertia Kg.m^2), B: Rotor Friction (Nm/(rad/s)).

From the DC motor model (Equation in 19 and 20), the motor current and angular velocity were first determined. Subsequently, the torque value was calculated. The torque generated by each reaction wheel along the x, y, and z axes is expressed as follows[24]:

$$\begin{bmatrix} T_{c,x} \\ T_{c,y} \\ T_{c,z} \end{bmatrix} = L \begin{bmatrix} \dot{H}_{RW1} \\ \dot{H}_{RW2} \\ \dot{H}_{RW3} \\ \dot{H}_{RW4} \end{bmatrix} \quad (21)$$

The block diagram of the angular velocity and torque control for the DC motors driving each of the four reaction wheels of the satellite is shown in Figure 4.

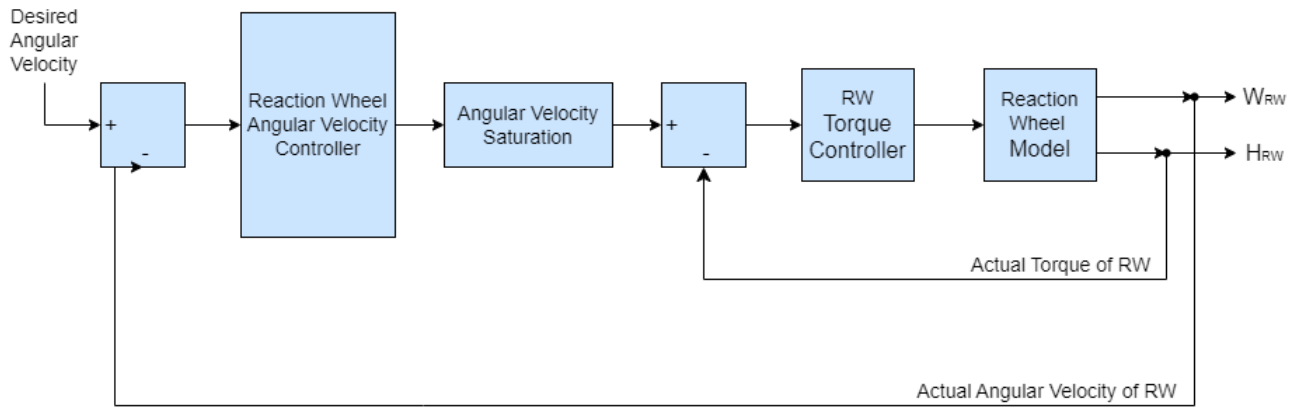

Figure 4. Cascade control of reaction wheel block diagram of LEO

A PID controller consists of three parameters: Kp, Ki, and Kd. The proportional controller (Kp) helps decrease the rise time and minimizes steady-state error. The integral controller (Ki) eliminates the steady-state error; however, it can lead to increased overshoot and settling time. The derivative controller (Kd) enhances system stability and helps reduce overshoot. In this study, the optimal PID gains are determined through MATLAB's auto-tuning feature in the PID block. As seen in the block diagram in Figure 4, the outer loop controller minimizes the difference between the desired angular velocity and the actual angular velocity of the motor comes from reaction wheel model. It determines the optimal PID controller gain parameters and generates the required torque value. Here, the desired angular velocity is provided as an output from the satellite attitude controller. The inner loop controller minimizes the difference between the desired torque and the actual torque obtained from the motor model. Using the optimized PID gain parameters, it generates the reference voltage value for each motor.

Figure 5 shows the angular velocity for each reaction wheel of satellite taken from the output of the reaction wheel model in the block diagram. Figure 6 shows the torque generated by each reaction wheel of satellite comes from the output of the reaction model in the block diagram. The settling time of angular velocity PID controller is 0.417 seconds while the settling time of torque PID controller is equal to 0.258 seconds.

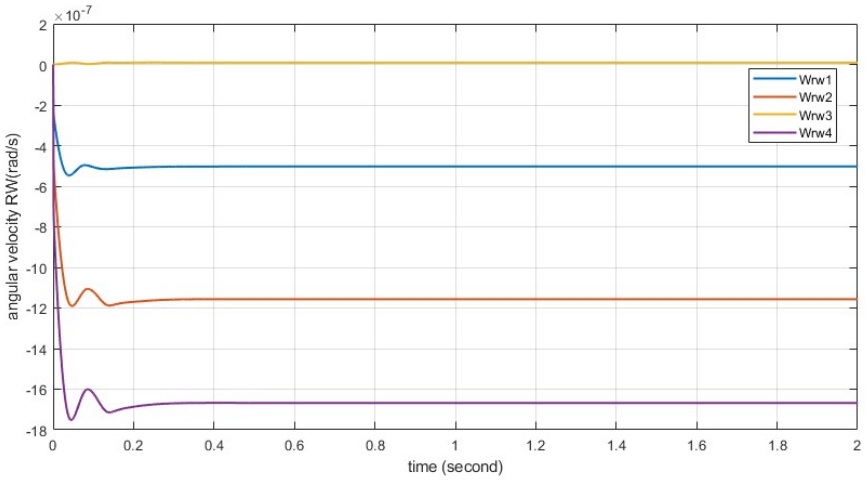

Figure 5. Angular velocity for each reaction wheel of satellite

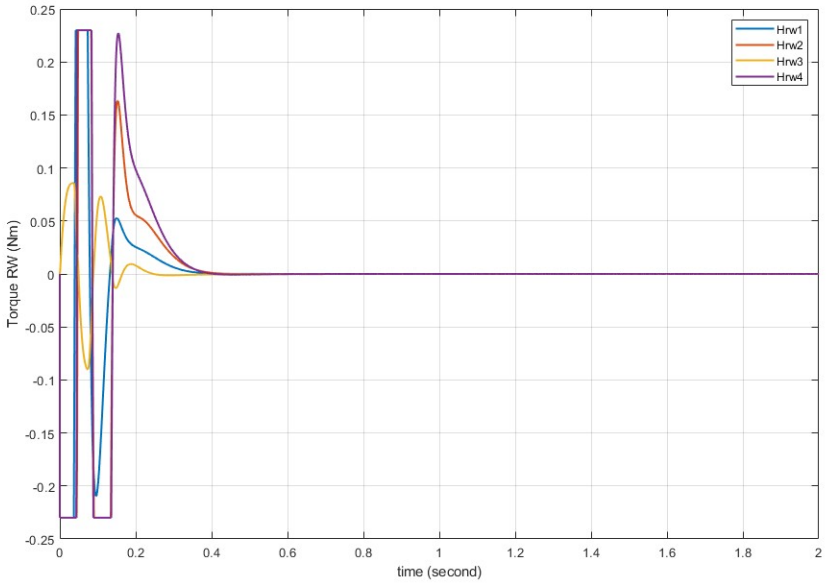

Figure 6. Torques generated by each reaction wheel of satellite

5.1. Control of Attitude LEO Satellite

From the satellite attitude model, the satellite's angular velocities, quaternion parameters, and Euler angles (roll, pitch, and yaw) were obtained. Using these parameters, the satellite's attitude angles were estimated through the integrated navigation system. The difference between the estimated attitude and the reference attitude was minimized, and the satellite's attitude was controlled using a PID controller with optimized gain coefficients.

The Simulink design, which includes the satellite attitude model consisting of the satellite's kinematic and dynamic equations given in section 3, reaction wheel controllers, and satellite attitude controllers, is shown in Figures 7 and Figure 8.

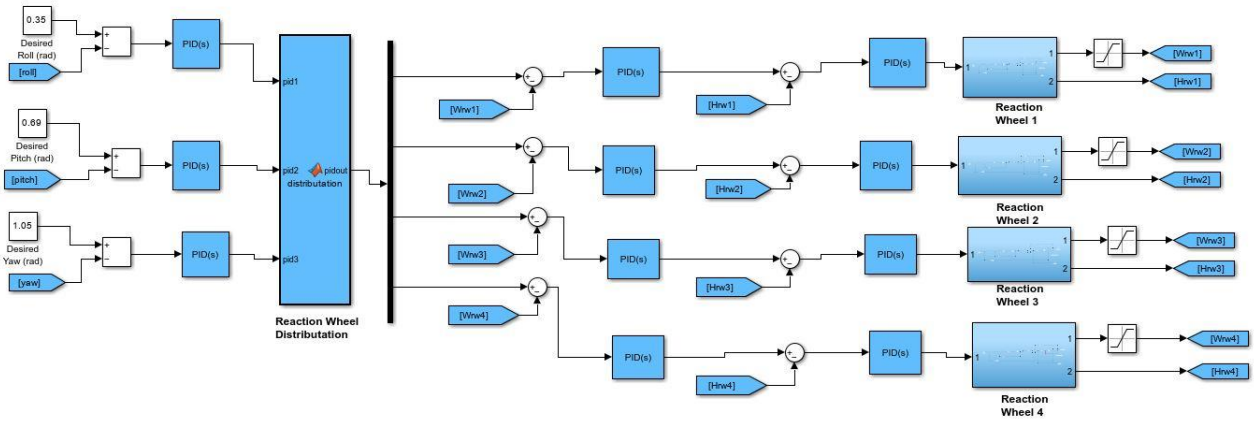

Figure 7. Simulink design for LEO attitude control, reaction wheel control

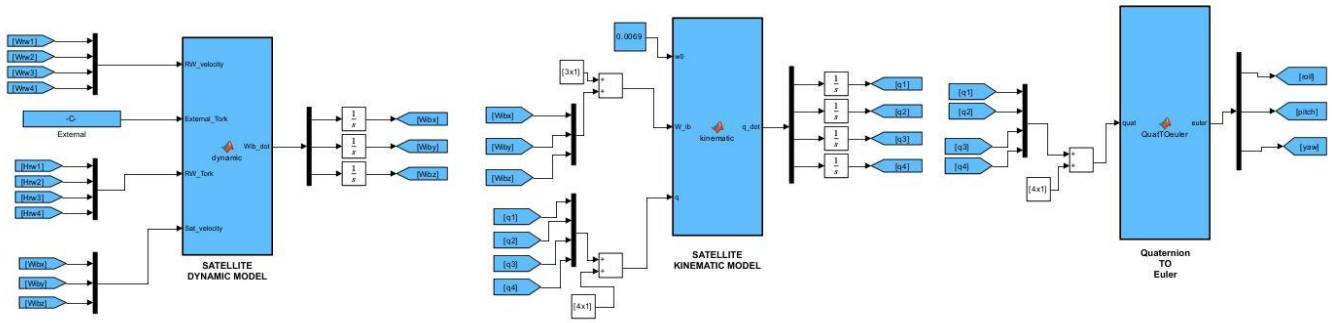

Figure 8. Simulink design for satellite attitude dynamic and kinematic model

In the implemented Simulink design, the desired roll, pitch and yaw angle is set 0.35 radian (20 degree), 0.69 radian (40 degree) and 1.05 radian (60 degree) respectively and the initial attitude value is set to zero. The satellite's reference roll, pitch, yaw angles (red line) and actual roll, pitch, yaw angles come from satellite attitude model (blue line) are shown in Figure 9, Figure 10 and Figure 11 respectively. The settling time of attitude PID controller 0.151 seconds. This controller response is obtained with 8.09e-7 for the proportional gain Kp, 1.08e-5 for the integral gain Ki and 1.3e-8 for the derivative gain Kd.

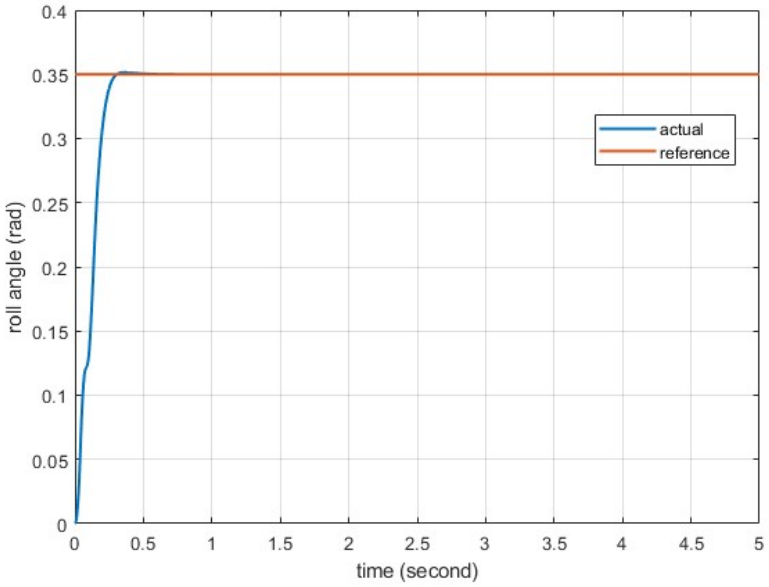

Figure 9. Reference roll angle and actual roll angle comes from satellite model

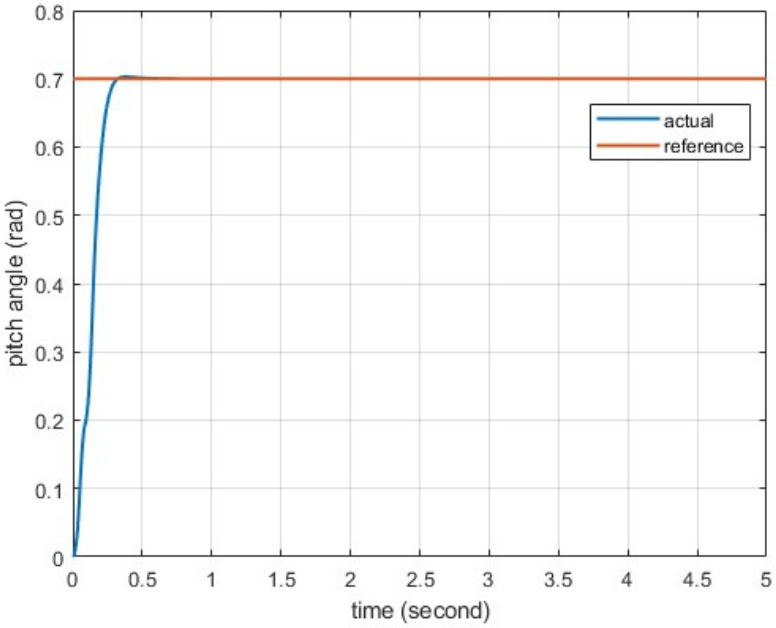

Figure 10. Reference pitch angle and actual pitch angle comes from satellite model

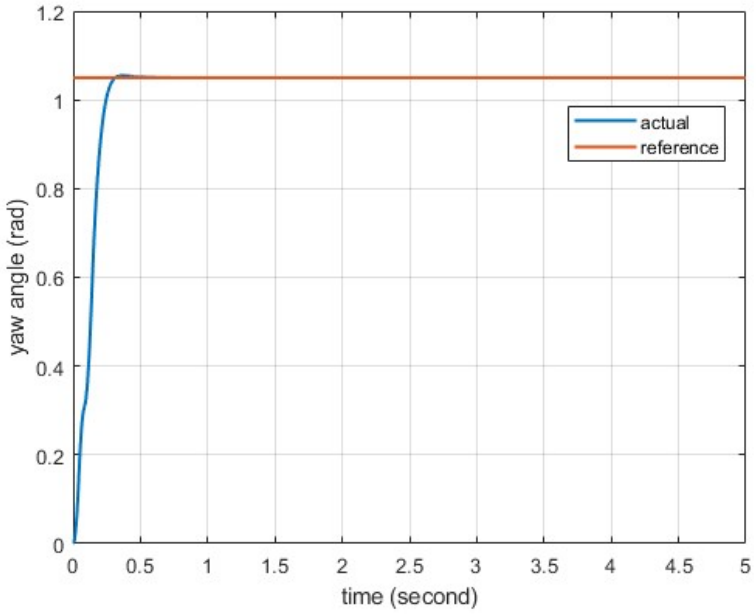

Figure 11. Reference yaw angle and actual yaw angle comes from satellite model

As seen in Figure 9, Figure 10 and Figure 11, the attitude of satellite achieves the target value within 0.1 seconds.

6. Navigation system of Low Earth Orbit Satellite

INS/GPS integration in the navigation of low Earth orbit (LEO) satellites is a critical technique, particularly for achieving high-precision attitude and position determination. The inertial navigation system (INS) is a system that measures the satellite's motion and orientation, continuously calculating position and velocity data using inputs from accelerometers and gyroscopes. However, the primary drawback of INS is the drift problem, where errors accumulate over time, making long-term navigation challenging. The global positioning system (GPS) serves as an external reference, continuously correcting the satellite's position and velocity errors. GPS data is used to compensate for INS errors and enhance navigation accuracy. LEO satellites operate in a rapidly changing navigation environment due to atmospheric effects and orbital acceleration, necessitating comprehensive integration. Techniques such as Kalman filtering process both INS and GPS data, leveraging the strengths of each system to ensure long-term accuracy while also providing highly precise short-term attitude and position information. As a result, INS/GPS integration significantly improves the accuracy of satellite position and orientation data, offering more reliable navigation for operational missions. In this study, the satellite's navigation is represented by the estimation of angular position information, specifically the roll, pitch, and yaw orientations.

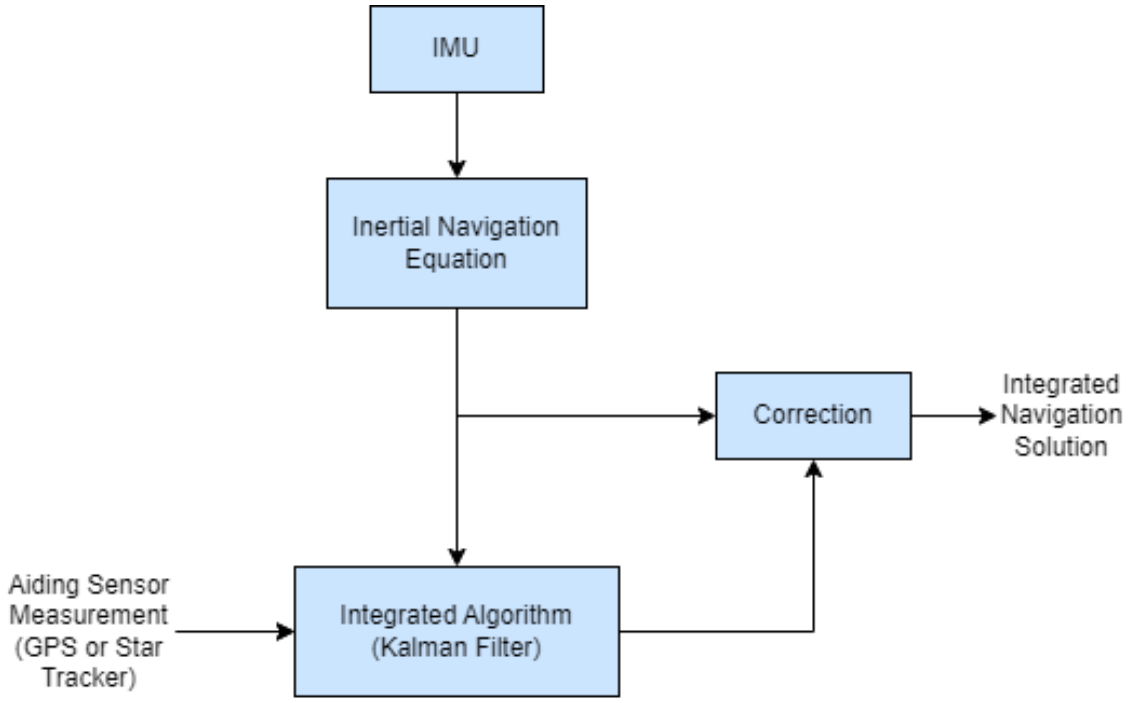

Figure 12. Block diagram of integrated navigation system of LEO

6.1. INS/GPS INTEGRATION

The INS/GPS integration model enhances the accuracy and reliability of position and velocity estimation by combining inertial navigation system (INS) and GPS data. Since the INS is integrated into the satellite, the INS/GPS integration model, which includes the dynamic equations of the INS, are used to improve system precision and perform error corrections. INS generates velocity, position, and orientation information by integrating acceleration and angular velocity data from gyroscopes and accelerometers. However, due to accumulated drift over time, it cannot provide sufficient accuracy on its own. Such errors are modeled using dynamic equations such as the position error derivative and velocity error derivative. In this study, the satellite's attitude states were estimated using an extended Kalman filter as the estimation algorithm. The error state vector that forms the system model of the extended Kalman filter were defined in the ECEF frame, including attitude, velocity, position information, and the bias errors of the inertial measurement unit, as shown in Equation 22[23]. This study focuses on the estimation of the satellite's attitude data.

$$x_{eb}^{e} = [\delta\varphi_{eb}^{e} \quad \delta v_{eb}^{e} \quad \delta r_{eb}^{e} \quad b_a \quad b_g]^T \tag{22}$$

Here, $\delta\varphi_{eb}^{e}$represents the attitude error vector, δv_{eb}^{e}denotes the velocity error vector, and δr_{eb}^{e}corresponds to the position error vector. Additionally, $b_a$refers to the accelerometer bias error vector, while b_g, represents the gyroscope bias error vector.

The time-dependent variation of the attitude error, $\delta\dot{\varphi}_{eb}^{e}$is given in Equation 23. In this equation, $\hat{C}_{b}^{e}$represents the transformation matrix, and Ω_{ie}^{e}denotes the skew-symmetric matrix of the Earth's angular velocity [22].

$$\delta\dot{\varphi}_{eb}^{e} = \hat{C}_{b}^{e} b_{g} - \Omega_{ie}^{e}\delta\varphi_{eb}^{e} \tag{23}$$

The time-dependent variation of the velocity error is given below.

$$\delta\dot{v}_{eb}^{e} = \hat{C}_{b}^{e} b_{a} - \left(\hat{C}_{b}^{e}\hat{f}_{ib}^{b}\right)\wedge\delta\varphi_{eb}^{e} - 2\Omega_{ie}^{e}\delta v_{eb}^{e} \tag{24}$$

In the equation, $\hat{f}_{ib}^{b}$represents the estimated acceleration (force) while δv_{eb}^{e}denotes the satellite velocity error [22].

The time-dependent variation of the position error, $\delta\dot{r}_{eb}^{e}$is presented in Equation 25

$$\delta\dot{r}_{eb}^{e} = \delta v_{eb}^{e} \tag{25}$$

The state-space model of the system is given in Equation 26[22].

$$\dot{x} = Ax + Bw \tag{26}$$

Here, w represents the system noise and is defined as zero-mean Gaussian noise. A denotes the system matrix, while B represents the system covariance matrix. The system matrix is defined in Equation 27 based on the system states.

$$A = \begin{bmatrix} -\Omega_{ie}^{e} & 0_3 & 0_3 & 0_3 & \hat{C}_{b}^{e} \\ \left[-\hat{C}_{b}^{e} f_{ib}^{b}\wedge\right] & -2\Omega_{ie}^{e} & 0_3 & \hat{C}_{b}^{e} & 0_3 \\ 0_3 & I_3 & 0_3 & 0_3 & 0_3 \\ 0_3 & 0_3 & 0_3 & 0_3 & 0_3 \\ 0_3 & 0_3 & 0_3 & 0_3 & 0_3 \\ 0_3 & 0_3 & 0_3 & 0_3 & 0_3 \end{bmatrix} \tag{27}$$

The system noise covariance matrix is given in Equation 28 [22].

$$B = \begin{bmatrix} n_{rg}^{2} I_3 & 0_3 & 0_3 & 0_3 & 0_3 \\ 0_3 & n_{ra}^{2} I_3 & 0_3 & 0_3 & 0_3 \\ 0_3 & 0_3 & 0_3 & 0_3 & 0_3 \\ 0_3 & 0_3 & 0_3 & 0_3 & 0_3 \\ 0_3 & 0_3 & 0_3 & n_{bad}^{2} I_3 & 0_3 \\ 0_3 & 0_3 & 0_3 & 0_3 & n_{bgd}^{2} I_3 \end{bmatrix} \tag{28}$$

Here, $n_{rg}^2, n_{ra}^2, n_{bad}^2, n_{bgd}^2$represent the random noise power density of the gyroscope and accelerometer, as well as the bias error power density of the accelerometer and gyroscope, respectively. σ_{ra}, σ_{rg}denote the standard deviations of noise in force measurement for the accelerometer and angular velocity measurement for the gyroscope, respectively. $\tau_i$represents the integration time interval, while $\sigma_{bad}$and σ_{bgd} correspond to the bias deviations of the accelerometer and gyroscope [22]. Since the inertial sensor data used in the navigation system is sampled at discrete time points, the discrete-time equivalents of the continuous system and the measurement model must be established [22].

$$x_{k+1} = \emptyset_k x_k + w_k \tag{29}$$

Here, $\emptyset_k$represents the transition matrix, which is expressed in Equation 30 under the assumption that the system dynamics matrix A remains constant over the time interval $\Delta t_{k+1} - t_k$. Higher-order terms beyond the second degree have been neglected.

$$\emptyset_k(\mathrm{t}) = e^{A\Delta t} = I + At + \frac{(A\Delta t)^2}{2!} \tag{30}$$

The measurement model consists of the satellite's attitude errors. It is assumed that the attitude information is obtained from the onboard GPS and IMU. In this study, the second sensor for attitude data, apart from the IMU, was assumed to be obtained from GPS. Instead of this GPS data, attitude-measuring sensor data such as a star tracker can also be considered, making the INS/GPS model applicable in this context.Since the measurements are collected at discrete intervals, the measurement vector is represented as:

$$z_k = H_k + n_k \tag{31}$$

Where H_k is the measurement matrix selected with dimensions 3×15.n_k is noise source and kis measurement update iteration. The measurement data is generated through simulation by adding noise to the satellite attitude model. The measurement noise is considered as zero-mean Gaussian noise. The measurement matrix H_k is selected with dimensions 3×15.

The measurement innovation vector for the extended Kalman filter is given in Equation 32. In Equation 32, $\tilde{z}_{GPS}$ and $\tilde{z}_{IMU}$represent the GPS and IMU measurement data generated through simulation, respectively.

$$\delta z_k = \tilde{z}_{GPS} - \tilde{z}_{IMU} \tag{32}$$

The measurement covariance matrix is selected with dimensions 3×3 as given in Equation 33. R11 and R22 correspond to the measurement accuracy of the attitude.

$$R_k = \begin{bmatrix} R_{11} & zeros(3) \\ zeros\ (3) & R_{22} \end{bmatrix} \tag{33}$$

$$H_k = \begin{bmatrix} 1 & 0 & 0 & 0 & 0 & 0 & 0 & 0 & 0 & 0 & 0 & 0 & 0 & 0 & 0 \\ 0 & 1 & 0 & 0 & 0 & 0 & 0 & 0 & 0 & 0 & 0 & 0 & 0 & 0 & 0 \\ 0 & 0 & 1 & 0 & 0 & 0 & 0 & 0 & 0 & 0 & 0 & 0 & 0 & 0 & 0 \end{bmatrix} \tag{34}$$

Figure 13 shows the actual roll angle comes from satellite attitude model, sensor data such as IMU and GPS generated by adding noise to the satellite attitude model and the estimated roll angle data comes from integrated navigation system. Figure 14 shows the actual pitch angle comes from satellite attitude model, sensor data obtained by adding noise to the satellite attitude model and the estimated pitch angle data comes from integrated navigation system.

Figure 15 shows the actual yaw angle comes from satellite attitude model, sensor data generated by adding noise to the satellite attitude model and the estimated yaw angle data comes from integrated navigation system. As seen figures the estimated angle values are close to the actual values.

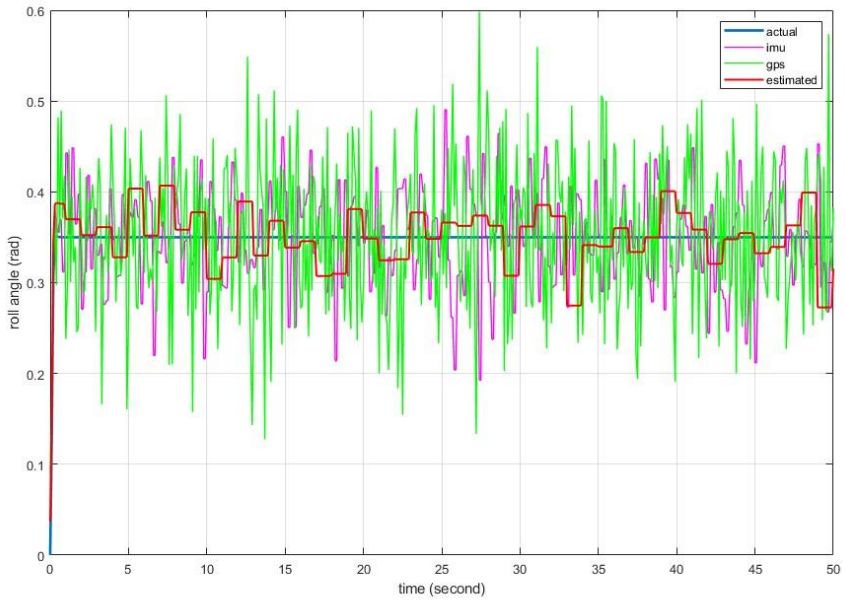

Figure 13. Actual roll angle comes from satellite model, measured roll angle comes from INS and GPS and estimated roll angle comes from integrated navigation system

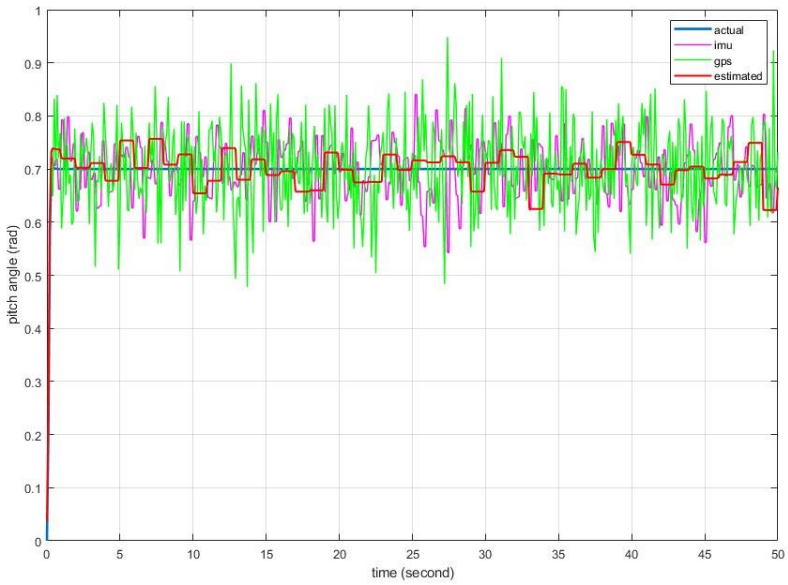

Figure 14. Actual pitch angle comes from satellite model, measured pitch angle comes from INS and GPS and estimated pitch angle comes from integrated navigation system

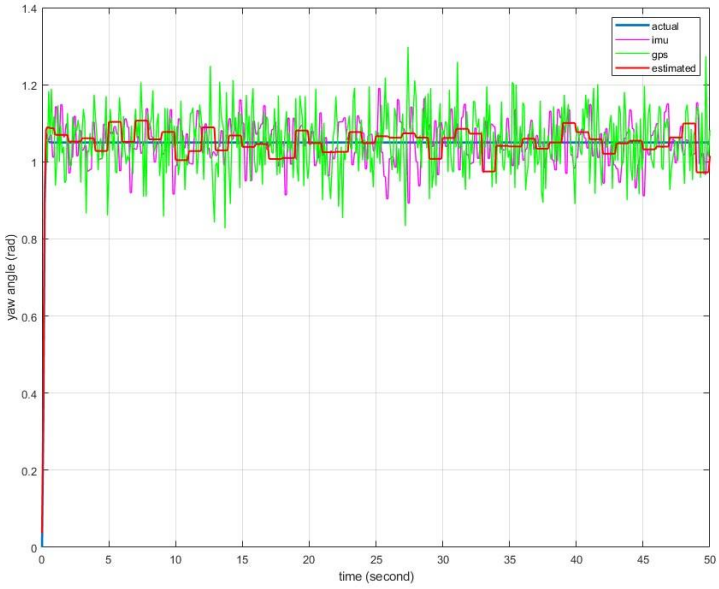

Figure 15. Actual yaw angle comes from satellite model, measured yaw angle comes from INS and GPS and estimated yaw angle comes from integrated navigation system

7. Conclusion

In this study, the orbit and attitude model of a low Earth orbit satellite has been developed. The attitude model has been addressed both dynamically and kinematically, and the satellite's attitude has been expressed in terms of quaternion parameters and Euler angles. To successfully estimate the satellite's attitude information using the INS/GPS integrated navigation system, sensor data have been generated, and two different sensor datasets have been fused using an Extended Kalman Filter (EKF).

For satellite attitude control, a DC motor model driving the reaction wheels has been created, and the angular velocity and torque of the motor have been controlled. A PID controller has been designed, and the optimal gain coefficients have been determined to minimize the difference between the integrated navigation system output and the desired attitude information. Simulation results demonstrate that the PID controller successfully adjusts the satellite's attitude to the desired value in a very short time. Additionally, it has been confirmed that the INS/GPS-based navigation system, using the Extended Kalman Filter (EKF), successfully estimates the satellite's angular position and attitude.

References

[1] L. Shakun, N. Koshkin, E. Korobeynikova, D. Kozhukhov, O. Kozhukhov, S. Strakhova et al. Comparative analysis of global optical observability of satellites in LEO. Advances in Space Research. 2021, 67(6), 1743-1760.
[2] Lalbakhsh A., Pitcairn A., Mandal K. et al. Darkening Low-Earth Orbit Satellite Constellations: A Review. IEEE Access 2022, 41810(4), 24383-24394.
[3]G. Avanzini, E.L. de Angelis, F. Giulietti, N. Serrano et al. Attitude control of Low Earth Orbit satellites by reaction wheels and magnetic torquers. Acta Astronautica. 2019, 160, 625-634.
[4]Farhangian, F.; Benzerrouk, H.; Landry, R., Jr. et al. Opportunistic In-Flight INS Alignment Using LEO Satellites and a Rotatory, IMU Platform et al. Aerospace. 2021, 8, 280.
[5]F. S. Prol. Position, Navigation, and Timing (PNT) Through Low Earth Orbit (LEO) Satellites: A Survey on Current Status, Challenges, and Opportunities IEEE Access. 2022, 10, 83971-84002. 453
[6]Y. Hu, X. Zhang and L. Chen et al. Strategy Design and Sensor Scheduling for Optical Navigation of Low Earth Orbit Satellites, IEEE Sensors Journal. 2018, 18(23), 9802-9811.
[7]Ye, L.; Gao, N.; Yang, Y.; Deng, L.; Li, H. et al. Three Satellites Dynamic Switching Range Integrated Navigation and Positioning Algorithm with Clock Bias Cancellation and Altimeter Assistance. Aerospace. 2023, 10, 411.
[8]Ivanov, D.; Monakhova, U.; Guerman, A.; Ovchinnikov, M. et al. Decentralized Control of Nanosatellite Tetrahedral Formation Flying Using Aerodynamic Forces. Aerospace 2021, 8, 199.
[9]Dalbins, J., Allaje, K., Ehrpais, H., Iakubivskyi, I. et al. Interplanetary Student Nanospacecraft: Development of the LEO Demonstrator ESTCube-2. Aerospace. 2023, 10, 503.
[10]Daniel Calvo, TaisirAvilés, Victoria Lapuerta, Ana Laverón-Simavilla et al. Fuzzy attitude control for a nanosatellite in low Earth orbit, Expert Systems with Applications. Acta Astronautica. 2016, 58, 102-118.
[11]Boussadia, H.; Si Mohammed, A.M.; Boughanmi, N.; Meche, A. et al. Sliding Mode Control Based on Backstepping Approach for Microsatellite Attitude Pointing. Eng. Proc. 2022, 14(24).
[12]Ivanov, D.; Monakhova, U.; Guerman, A.; Ovchinnikov, M. et al. Decentralized Control of Nanosatellite Tetrahedral Formation Flying Using Aerodynamic Forces. Aerospace 2021, 8, 199.
[13]Sandu, C.; Silivestru, V.; Cican, G.; S, erbescu, H.; Tipa, T.; Totu, A.; Radu, A. et al. On a New Type of Combined Solar Thermal/Cold Gas Propulsion System Used for LEO Satellite's Attitude Control. Appl. Sci. 2020, 10, 7197.
[14]G. Avanzini, E.L. de Angelis, F. Giulietti, N. Serrano et al. Attitude control of Low Earth Orbit satellites by reaction wheels and magnetic torquers. Acta Astronautica. 2019, 160, 625-634.

[15]H. A. Talebi, K. Khorasani and S. Tafazoli et al. A Recurrent Neural-Network-Based Sensor and Actuator Fault Detection and Isolation for Nonlinear Systems With Application to the Satellite's Attitude Control Subsystem. IEEE Transactions on Neural Networks. 2009, 20(1), 45-60.
[16]Zhou, Y., Li, J., Wang, H., Chen, Z. et al. Attitude Control of Small Satellites Using PID Controllers with Sensor Fusion Techniques. Aerospace Science and Technology. IEEE Journal on Miniaturization for Air and Space Systems. 2019, 85, 208-217.
[17]Fitzgerald, B., Keegan, C et al. Advanced Control Strategies for Spacecraft Attitude Management. Journal of Guidance, Control, and Dynamics. 2016, 39(7), 1534-1546.
[18]Sabine Klinkner, Steffen Gaiber, Jonas Keim et al. Stuttgart University's reliable, high-performance small satellite platform on its first mission "Flying Laptop. 12th IAA Symposium on small Satellites for Earth Observation. 2019.
[19]Turco, F., Traub, C., Gaißer, S. et al. Analysis of Collision Avoidance Manoeuvres Using Aerodynamic Drag for the Flying Laptop Satellite. Aerotec. Missili Spaz. 2024, 103, 61-71.
[20]KutluAykut. Design of Kalman Filter Based Attitude Determination Algorithms for a LEO Satellite and for a Satellite Attitude Control Test Setup. Bachelors degree thesis, METU 2008.
[21]KarataşSoner. Dynamic Modelling, Sımulatıons and Some Nonlinear Attitude Control Techniques. Bachelors degree thesis, METU, 2006.
[22]Efendioglu Gamze. Design of Kalman Filter based Attitute Determination and Control Algorithms for a LEO Satellite. Bachelors degree thesis, METU 2019.
[23]Kaplan Ceren. LEO Satellites: Attitude Determination and Control Components; Some Linear Attitude Control Techniques. Bachelors degree thesis, Middle East Technical University.2006.
[24] Kök ˙Ibrahim. Comparison and Analysis of Attitude Control Systems of a Satellite Using Reaction Wheel Actuators. Bachelorsdegree thesis, Lulea University of Technology.2012.